공학석사학위논문

Wave-Structure Interaction Analysis of a Submerged Floating Tunnel

파랑하중을 고려한 부유식 수중 터널의 유탄성 거동 해석

2022 년 2 월

서울대학교 대학원

건설환경공학부

김 수 민

Wave-Structure Interaction Analysis of a Submerged Floating Tunnel

파랑하중을 고려한 부유식 수중 터널의 유탄성 거동 해석

지도교수 김 호 경

이 논문을 공학석사 학위논문으로 제출함
2022년 2월

서울대학교 대학원
건설환경공학부
김 수 민

김수민의 공학석사 학위논문을 인준함
2021년 12월

위 원 장	채 윤 병	(인)
부 위 원 장	김 호 경	(인)
위 원	이 해 성	(인)

ABSTRACT

This study performs wave-structure interaction analysis of a submerged floating tunnel (SFT) with mooring lines and investigates the effect of structure parameters on dynamic responses under wave loads. Airy wave theory and Morison's Equation are used to calculate the wave force. The numerical model of SFT is verified by comparing it with the dynamic response of the experimental model studied by Oh et al. [5]. The effect of key design parameters (Buoyancy weight ratio, clearance, tether incline angle) on the performance of SFT under wave load is presented. Even though the SFT natural frequency and wave frequency were not close, Structure response amplification was observed for a particular range of the parameters. It was found that this amplification is due to the time-dependent fluctuating natural frequency of SFT. The results indicate that fluctuating natural frequency should be evaluated properly since severe displacement can occur in such a specific situation.

Keywords: Submerged floating tunnel, Wave-structure interaction, Buoyancy-weight ratio, Clearance, Response amplification

Student Number: 2020-29808

TABLE OF CONTENTS

LIST OF FIGURES

LIST OF TABLES

CHAPTER 1

INTRODUCTION

1.1 Research Background

Recently, the interest in Submerged Floating Tunnel (SFT) has increased as structure engineers search for a new transportation concept for crossing sea straits in relatively long-distance and deep-water sites. The SFT system maintains its balance by buoyancy, self-weight, and tension of mooring lines. SFT can be an alternative to the conventional long-span bridges by overcoming the existing limitations. The main advantages of SFT are construction cost per unit length is relatively irreverent to a tunnel length, the ship traffic problem can be solved, and an optimal design can be safe against both waves and earthquakes [1]. Also, SFT is relatively easy to construct compared to existing marine transportation facilities, which are very difficult to construct under the sea and cause severe environmental pollution [2].

Despite the numerous advantages, due to technological challenges, lack of safety assurance, and political issues, there is no developed SFT project in the world yet [3, 4]. Therefore, it is necessary to accurately understand the behavioral characteristics under various environmental loads to construct an actual SFT.

Numerous researches have been conducted on the behavior of SFT so far. Oh et al. [5, 6] and Yang et al. [7] conducted experimental studies on the behavior of the tunnel and mooring line tension. A scaled SFT model is applied in the wave flume with regular waves. Furthermore, Won et al. [8] conducted a wave tank experiment to evaluate dual SFT section motion under wave force. Scaled wave flume experiments were limited in terms of cost, time, and parameter adjustment.

In order to make a numerical model of SFT, it is important to define the correct wave force. Currently, there are two major methods for determining the hydrodynamic wave load of SFTs, including Morison's equation and diffraction theory [9, 10]. Estimating these two methods by Kunisu et al. [11] for the hydrodynamic computation of SFTs was performed. It was found that in normal construction conditions, both the drag and inertial forces account for significant proportions. Cifuentes et al. [12] also used two independent numerical simulation methods and confirmed that both methods determining wave load give good agreement with wave flume experimental result.

Many types of research evaluated the SFT behavior under different structural parameters. Long et al. [3, 13] evaluated structural responses with different buoyancy weight ratios. Also, the effects of the inclined mooring angle on the dynamic responses of SFT were analyzed by Chen et al. [14]. In particular, the computational fluid dynamic analysis was performed very

similarly to the real environment by performing a real-time flow field analysis, rather than simply defining the wave load by the Morison equation.

In addition to the SFT analysis focusing on the wave load, experimental study of vortex-induced vibration [15] and drag force [16] in ocean current, dynamic response analysis due to fluid-vehicle-tunnel interaction [17], slack analysis of mooring lines [18, 19], the effect of accidental impact load [20, 21], and seismic analysis of SFT were performed [22].

On the other hand, only a few research articles deal with the SFT response amplification phenomenon due to propagating waves. Chen et al. [14] pointed out that response amplification is found in a specific mooring angle range and emphasized that such mooring line angle should be avoided in the design of SFTs. However, the cause of this phenomenon has not been determined. It is hard to judge if this response amplification is simply a resonance with SFT natural frequency and wave frequency because the two frequency does not get close in the focused range. It is necessary to understand the response amplification phenomenon well and determine the exact cause since this can cause serious damage to SFT.

1.2 Research Objective and Layout

This research aims to understand the wave-structure behavior of SFT under various loading conditions and different structural parameters. An additional object is to investigate the cause of the SFT response amplification when the fluctuating structural natural frequency gets close to wave frequency under specific conditions.

The general layout is as follows. Chapter 2 describes in detail the numerical model. The Airy linear wave theory and Morison's Equation are two basic theories derived by flow potential theory. Governing Equation of the SFT system is also derived, and a brief explanation of the numerical model is presented. In Chapter 3, validation of the numerical model is discussed. The validation is done by comparing the numerical analysis result with the theoretical solution and scaled experiment result performed by Oh et al. [5]. Finally, the effect of key design parameters (Buoyancy weight ratio, clearance, tether incline angle) on the performance of SFT under wave load is presented. The structure response amplification range for each parameter is presented, and the cause of this phenomenon is discussed.

CHAPTER 2

DESCRIPTION OF NUMERICAL MODEL

2.1 Theoretical background

2.1.1 Airy linear wave theory

Hydrodynamic loads that are mainly dealt with in the design and analysis of offshore structures are forces induced by waves and current. In general, the current load considers the behavior of water particles moving at a constant velocity in a specific direction rather than causing the dynamic motion of the fluid. On the other hand, wave load causes the rotational motion of water particles below the free surface of the water. The dynamic movement of water particles by waves continuously induces a change in fluid pressure on the surface of the floating structure. This dynamic pressure excites the floating structure, causing a dynamic response. Therefore, it is important to understand the motion of water particles below the free surface and establish it mathematically for a specific wave component. The velocity and acceleration of water particles can be obtained by understanding the motion of water particles. Consequentially, the hydrodynamic force acting on the floating structure is calculated to enable wave-structure interaction analysis.

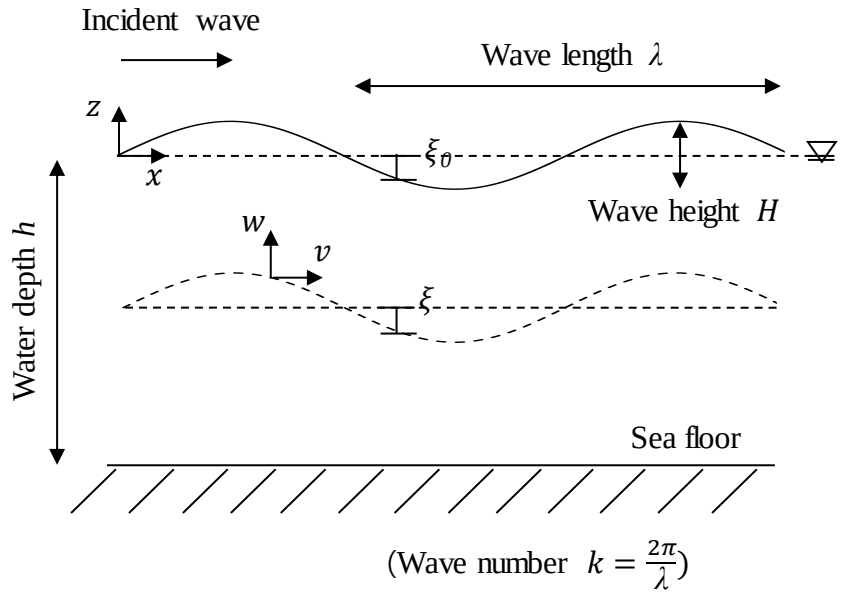

Figure 2.1. Notation for defining Airy linear wave theory

Regular waves can be defined through the Airy wave theory based on the wave potential theory. For any small volume in a flow field, the continuity equation is defined by the law of conservation of mass and by assuming incompressible fluid. In this continuity equation, if there is no frictional force of water and the assumption of non-rotational fluid is applied, the irrotationality condition can be defined as Equation (2.1),

$$\vec{\nabla} \times \vec{V} = 0 \; (curl\, \vec{V} = 0) \tag{2.1}$$

where $\vec{\nabla}$ is the gradient vector and $\vec{V}$ is the fluid velocity vector. A logical

consequence of this condition is the existence of a velocity potential $\Phi(x,z)$. For an incompressible homogeneous fluid, substituting the velocity vector in terms of the potential Φ, the incompressible inviscid fluid is governed by:

$$\vec{\nabla}^2\Phi = \frac{\partial^2\Phi}{\partial x^2} + \frac{\partial^2\Phi}{\partial z^2} = 0 \tag{2.2}$$

The first boundary condition is defined as zero vertical velocity at seafloor shown in Equation (2.3),

$$w = \frac{\partial\Phi}{\partial z}\Big|_{z=-h} = 0 \tag{2.3}$$

where w is the water particle's vertical speed, and h is sea level height. The second boundary condition is defined as zero pressure at sea level shown in Equation (2.4),

$$-\frac{1}{\rho}\frac{\partial p}{\partial x} = \frac{\partial v}{\partial t} + v\frac{\partial v}{\partial x} + w\frac{\partial v}{\partial z} \tag{2.4}$$

Based on the governing Equation and the two boundary conditions, the potential is derived as Equation (2.5).

$$\Phi = -\frac{H \cdot g \cdot \cosh k(z+h)}{2\omega \cdot \cosh kh} \sin(kx - \omega t) \tag{2.5}$$

In Equation (2.5), H is wave height, g is gravitational acceleration, x is the x-axis coordinate, z is the z-axis coordinate, k is wave number, ω is the angular frequency of the incident wave.

The motion of fluid particles in regular waves can be derived from the velocity potential obtained earlier. As a result, Equations (2.6) and (2.7) are x and z direction water particle velocity. The water particle acceleration is shown in Equations (2.8) and (2.9) can also be obtained by differentiating the obtained velocity.

$$v(x,z,t) = -\frac{\partial \Phi}{\partial x} = \frac{H \cdot g \cdot k \cdot \cosh k(z+h)}{2\omega \cdot \cosh kh} \cos(kx - \omega t) \tag{2.6}$$

$$w(x,z,t) = -\frac{\partial \Phi}{\partial z} = \frac{H \cdot g \cdot k \cdot \sinh k(z+h)}{2\omega \cdot \cosh(kh)} \sin(kx - \omega t) \tag{2.7}$$

$$\frac{\partial v}{\partial t} = \frac{H \cdot g \cdot k \cdot \cosh k(z+h)}{2\cosh kh} \sin(kx - \omega t) \tag{2.8}$$

$$\frac{\partial w}{\partial t} = -\frac{H \cdot g \cdot k \cdot \sinh k(z+h)}{2\cosh kh}\cos(kx - \omega t) \tag{2.9}$$

2.1.2 Morison's Equation

Morison et al. (1950) proposed an equation for expressing the total wave force as the sum of inertial and drag forces. The inertia force term is derived from the potential flow theory. First, C_M part, meaning the force of the fluid accelerated by a stationary object is proportional to the acceleration of the fluid. Second, the C_A part is an additional mass term that reflects the characteristic of moving the same volume of water occupied by the object when the structure moves. Accordingly, this term is proportional to the structure's acceleration. Lastly, the drag term consists of the square of the relative velocity of the fluid and the structure. An absolute value is entered to consider the direction of the incident wave.

Therefore, wave-induced load per unit length is defined by Morison's Equation (Equation (2.10)),

$$dF = \frac{\pi}{4}\rho D^2\{C_M \dot{v}_x(t) - C_A \ddot{u}(t)\} + \frac{1}{2}\rho D C_D (v_x - \dot{u}(t))|v_x - \dot{u}(t)| \tag{2.10}$$

where D is structure diameter, C_M is inertia coefficient, C_A is added mass coefficient, C_D is drag coefficient, u is structure displacement, z is target structure length. The total force can be obtained by integrating Equation (2.10) over the structure range as Equation (2.11).

$$\text{Total } F = \int \frac{\pi}{4}\rho D^2\{C_M \dot{v}_x(t) - C_A \ddot{u}(t)\} + \frac{1}{2}\rho D C_D (v_x - \dot{u}(t))|v_x - \dot{u}(t)|\, dz \tag{2.11}$$

Wave velocity, wave acceleration, structure velocity, and structure acceleration are all included in the defined wave load itself. In this aspect, the Equation of motion of the structure by the wave load is complicatedly defined.

2.2 Calculation of hydrodynamic load

The actual wave force received by the structure can be derived in two different ways. First, when the diameter of the structure is relatively small compared to the wave height (Equation 2.12), the effect of the movement of the structure itself on the wave can be neglected. For this case, Morrison's Equation defines wave forces in terms of inertia and drag.

The wave forces that a structure experiences are derived in two ways. First,

if the diameter of the structure(*D*) is relatively small compared to the wave height(*H*), the effect of the movement of the structure itself on the wave is negligible. For this case, the wave force can be obtained through Morison's Equation as shown in Equation (2.13), where F_I is inertia force and F_D is drag force

$$D < 3H \tag{2.12}$$

$$F = F_I + F_D \tag{2.13}$$

However, when the structure's diameter is relatively large compared to the wave height (Equation 2.14), the scattered wave generated by the movement of the structure is dominant. In this case, the wave force is defined by consideration of the restoring force, the radiational force, and the diffraction force, which is respectively F_{res}, F_{rad}, and F_{diff} as shown in Equation (2.15).

$$D > 3H \tag{2.14}$$

$$F = F_{res} + F_{rad} + F_{diff} \tag{2.15}$$

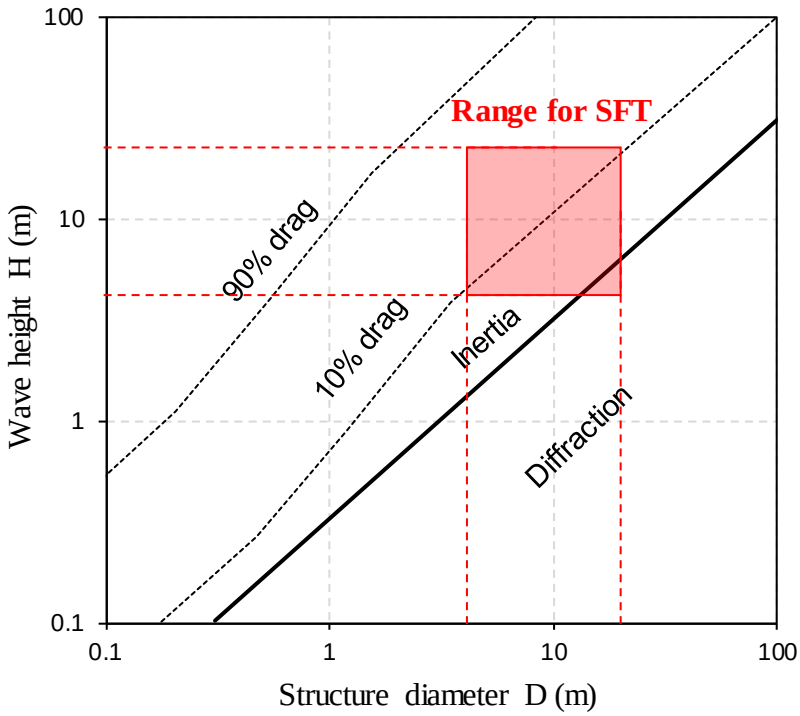

Figure 2.2. Loading regimes at still water level (Hogben et al. (1976))

Figure 2.2 shows which theory should be applied to calculate the wave force according to the structure's diameter and wave height. Referring to the preliminary design of SFT in previous studies, the minimum diameter when designing a one-lane tunnel is 4 m, and when designing a two-story four-lane tunnel, the maximum diameter is about 25 m. In addition, the design wave height range for offshore structures is 8m to 16m. Therefore, the SFT is included in the red region in Figure 2.2, and it is reasonable to apply Morison's Equation rather than the diffraction theory.

2.3 Governing Equation of wave-structure interaction

In order to perform a dynamic analysis of a structural system, it is important to formulate the governing equations of the system accurately. The SFT is statically in equilibrium by the buoyancy of the tunnel and the tension of the mooring lines. Also, as shown in Figure 2.3, the horizontal stiffness is defined by the p-delta effect. Therefore, the horizontal stiffness of the structure changes according to the initial tension of the mooring line, the total length of the mooring line, the elastic modulus, and the displacement of the tunnel.

The stiffness of the structure is derived through the free-body diagram as Equation (2.16) ~ (2.19).

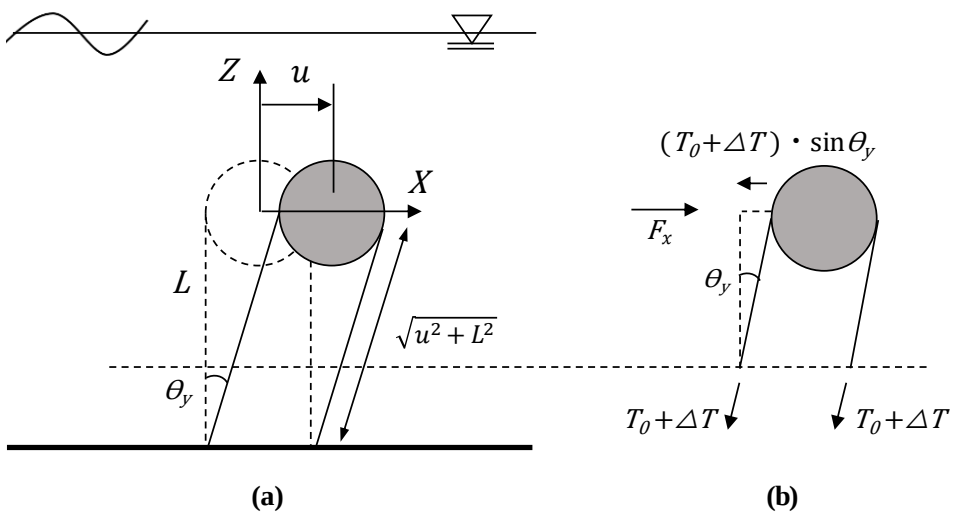

Figure 2.3. Schematic diagram (a) full model; (b) free-body diagram

$$\Delta T = (\sqrt{u^2(t) + L^2} - L) \cdot \frac{EA}{L} \tag{2.16}$$

$$F_x(t) = K_x \cdot u(t) \tag{2.17}$$

$$F_x(t) = 4 \cdot (T_0 + \Delta T) \cdot \sin\theta_y \tag{2.18}$$

$$\therefore K_x(t) = \frac{4 \cdot T_0}{\sqrt{u^2(t) + L^2}} + \frac{4 \cdot EA}{L} - \frac{4 \cdot EA}{\sqrt{u^2(t) + L^2}} \tag{2.19}$$

Where, $K_x(t)$ is lateral stiffness, $u(t)$ is tunnel lateral displacement, T_0 is initial mooring line tension, L is initial mooring line length, E is elastic modulus for mooring line, and A is cross section of mooring line.

In addition, the total mass of the structural system is defined as the sum of the mass of the tunnel itself and the added mass, which is a characteristic that the same volume of water must also move when the structure moves.

$$m_{added} = \frac{\pi D^2}{4} \cdot C_A \cdot L \tag{2.20}$$

$$m_{total} = m_{tunnel} + m_{added} \tag{2.21}$$

Therefore, the natural frequency of the SFT structure is expressed by time-dependent stiffness and total mass, as shown in Equation (2.22).

$$\omega_n = \sqrt{\frac{K_x(t)}{m_{total}}} \tag{2.22}$$

The governing Equation of SFT dynamic behavior is summarized in Equation (2.23) ~ (2.24). The second-order term of the structural velocity is generated by the drag term of the wave force. Despite the assumed undamped structural system, the damping term due to the wave force is generated. Structural stiffness is constantly changing with displacement. To solve this complex differential equation and calculate the structural response, a numerical approach was used using a commercial analysis program. Time-domain analysis was performed to reflect the change in the governing Equation according to the displacement of the structure.

$$m\ddot{u}(t) + c\dot{u}(t) + K_x u(t) = F \tag{2.23}$$

$$\therefore\ m_{total}\ddot{u}(t) + \frac{1}{2}\rho D C_D(\dot{u}(t) - v_x)|\dot{u}(t) - v_x| + K_x u(t) = A\rho C_M \dot{v}_x(t) \tag{2.24}$$

2.4 Description of numerical model

In this study, the SFT wave-structure interaction analysis was performed using ABAQUS/AQUA v6.14 (Time-series implicit dynamic analysis). Frame elements were used for all members. Timoshenko beam was used for the tunnel considering that the diameter is relatively large compared to the length, and incompressible truss elements were used for mooring lines to simulate cables properly. The initial shape analysis was performed by defining the mooring line's temperature load and introducing initial tension to the mooring line. The temperature change rate was calculated by Equation (2.25),

$$F_{buoyancy} - F_{tunnel} = 4 \cdot E \cdot A \cdot \alpha \cdot (\Delta T) \tag{2.25}$$

where α is the thermal expansion coefficient, and ΔT is the temperature change rate.

Considering that all members are frame elements, erection of the mooring line and the tunnel connection part is necessary. The connection between the tunnel and mooring line was modeled by introducing a member with zero mass with an elastic modulus of 1000 times or more. Hinge support was used as the boundary condition between the seabed and the mooring line. The details of the model are given in Table 2.1 and Figure 2.4.

Table 2.1. Main parameter values for SFT

Parameters	Values
Tunnel diameter	23 m
Tunnel thickness	0.275 m
Tunnel length	98 m
Tunnel density	10581 kg/m^3
Tunnel Elastic modulus	2E+11 Pa
Tether diameter	0.36 m
Tether area	0.1018 m^2
Tether length	68.5 m
Tether Elastic modulus	1.97E+11 Pa
Tether Density	8000 kg/m^3

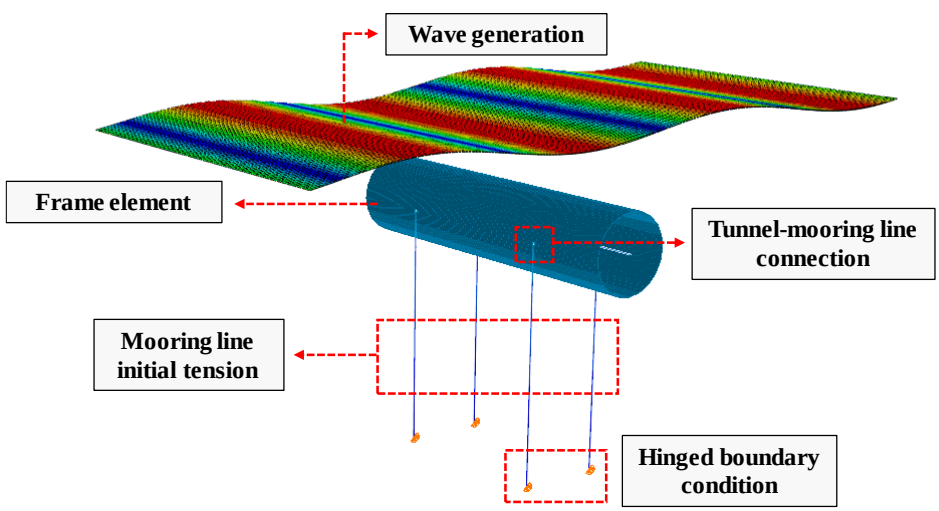

Figure 2.4. Details for SFT analysis model

CHAPTER 3

VERIFICATION OF NUMERICAL ANALYSIS

3.1 Verification of wave force application

To verify whether the analysis program accurately calculates the wave velocity, acceleration, and wave force, the exact solution calculated using Airy wave theory and Morison's Equation was compared with numerical analysis structural response. A fixed vertical pipe (Figure 3.1) was assumed, and the wave characteristics were defined as arbitrary waveforms without considering correlation (Table 3.1).

Table 3.1. Environmental conditions for vertical pipe

Parameters	Values
Wavelength (λ)	7 m
Wave period (T)	2.12 s
Wave height (H)	0.1 m
Water depth (h)	44 m
Structure diameter (D)	0.2 m

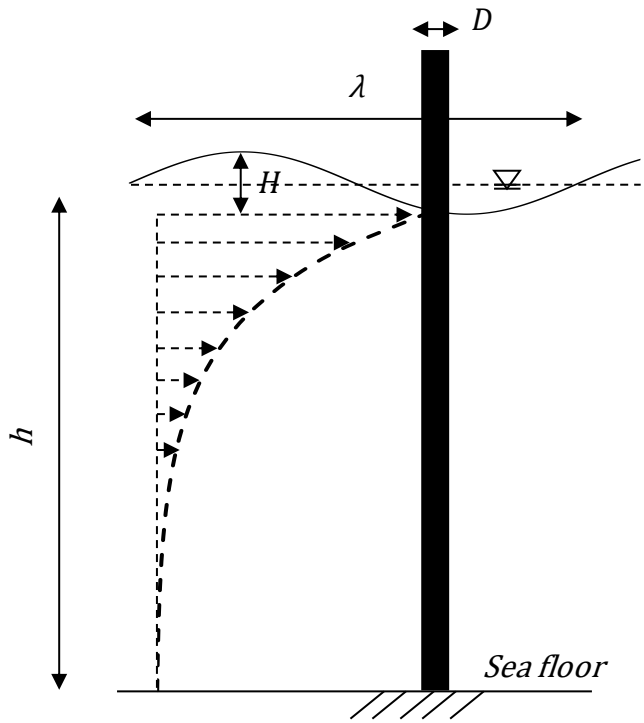

Figure 3.1. Schematic diagram of vertical pipe for load verification

As a result of the verification (Figure 3.2), it was confirmed that the numerical analysis result for the wave height, drag force, and inertia force component force all match well with the exact solution.

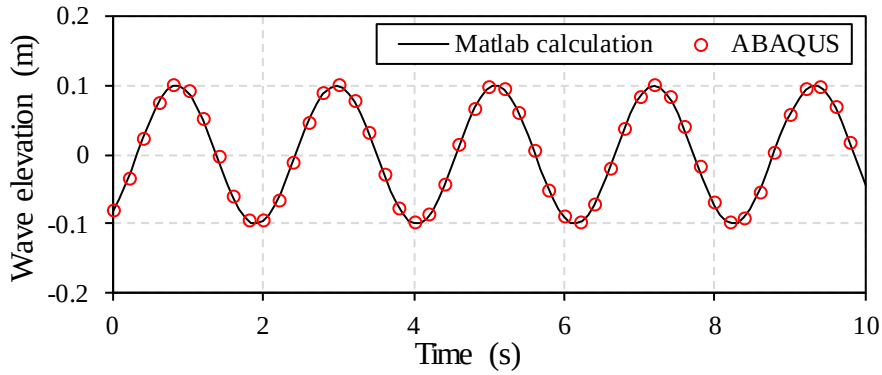

(a)

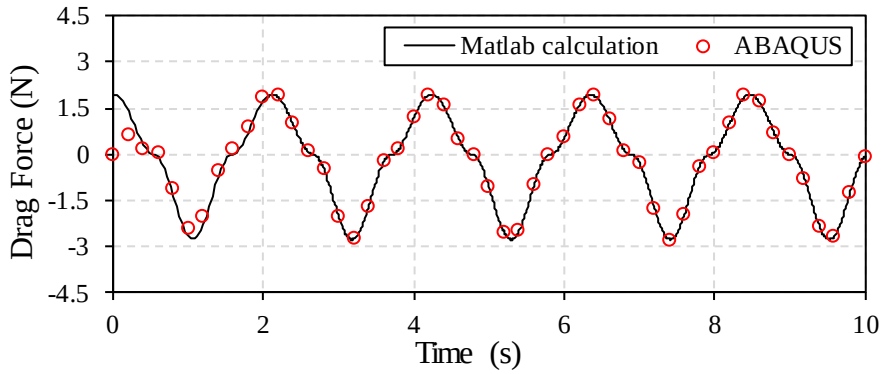

(b)

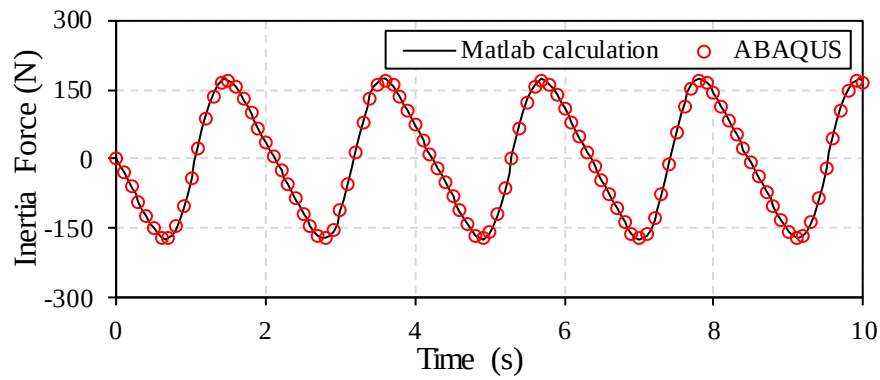

(c)

Figure 3.2. Verification of numerical model (a) wave elevation; (b) drag force; (c) inertia force

3.2 Verification of wave-structure interaction

For the SFT to be constructed, the displacement of the tunnel and the tension force for the mooring line in various environmental conditions is the main issue. Since there is no existing SFT so far, the scaled experiment conducted by Oh et al. (2013) was referred. The prototype SFT is a cylindrical structure with a length of 98.0 m and a diameter of 23.0 m (Figure 3.4). The hydrodynamic performance of SFT under wave loading was tested with a 1/100 scaled model in a wave flume, as shown in Figure 3.3. In the experimental study, a single periodic regular wave was generated in the tank. The motion of the tunnel and the tension of the mooring line were measured through image processing techniques and load cells.

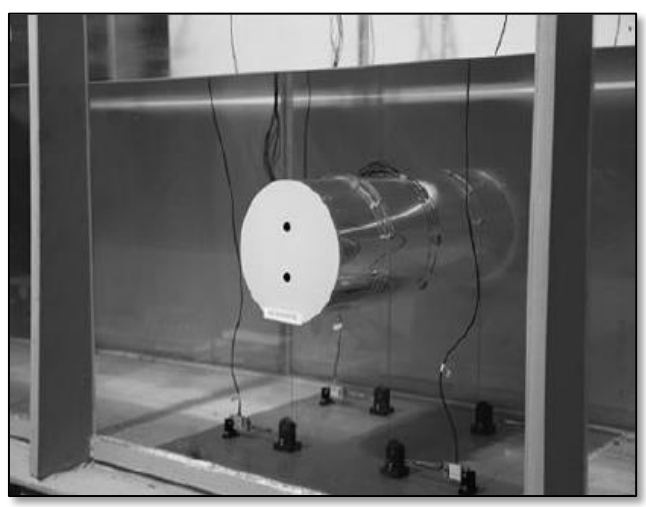

Figure 3.3. General view of the experimental setup (Oh et al. (2013))

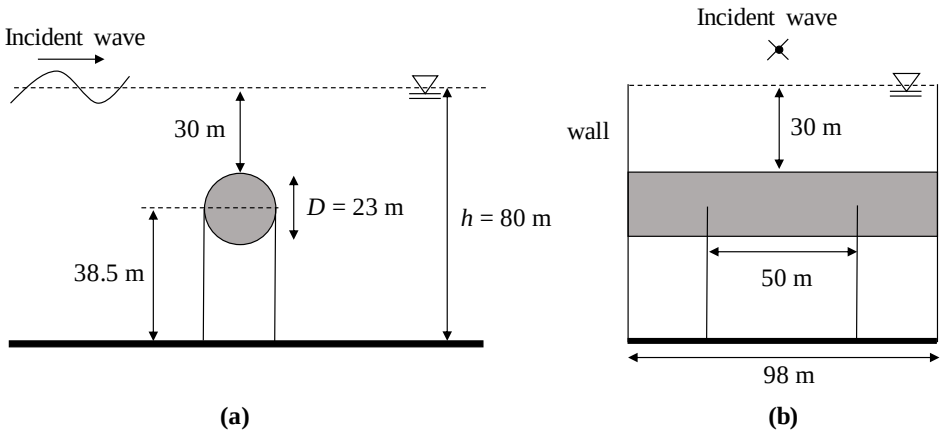

Figure 3.4. Schematic sketch for experimental study

(a) front view; (b) side view

The applied regular wave characteristic is shown in Table 3.2. The period of the wave and the slope of the wave are independent variables, and the wavelength is determined by the dispersion relationship (Equation (3.1)), which is derived through Airy linear wave theory.

$$\omega^2 = g \cdot k \cdot \tanh(kh) \tag{3.1}$$

The wave height is proportional to the wavelength according to the slope of the wave, as shown in Equation (3.2), where s denotes the wave slope.

$$s = \frac{H}{\lambda} \tag{3.2}$$

Table 3.2. Wave characteristic case

	Wave period, T (s)	**Wavelength, λ (m)**	**Wave steepness, s**	**Wave height, H (m)**
Case 1	10	156	0.013	2.03
			0.027	4.21
			0.040	6.24
			0.053	8.27
Case 2	13	254	0.013	3.30
			0.027	6.86
			0.040	10.16
			0.053	13.46

The verification result of the analysis model is shown in Figure 3.5 and Figure 3.6. The tunnel's sway motion, heave motion, and mooring line's tension are displayed for wave periods of 10 and 13 seconds. All graphs show maximum and minimum responses of the structure according to the change in wave height.

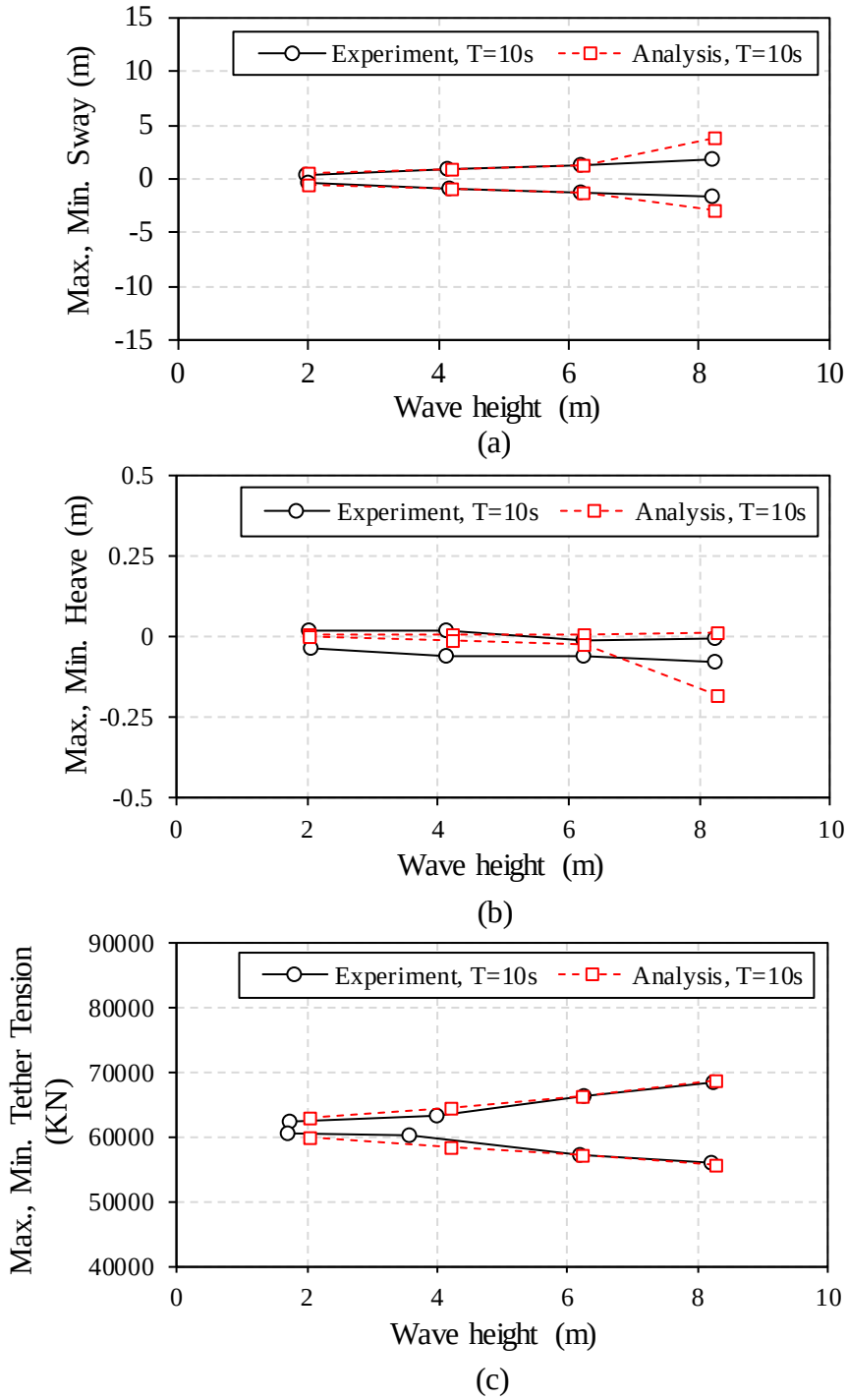

Figure 3.5. SFT response as function of wave height (T=10 s)

(a) sway motion; (b) heave motion; (c) tether tension

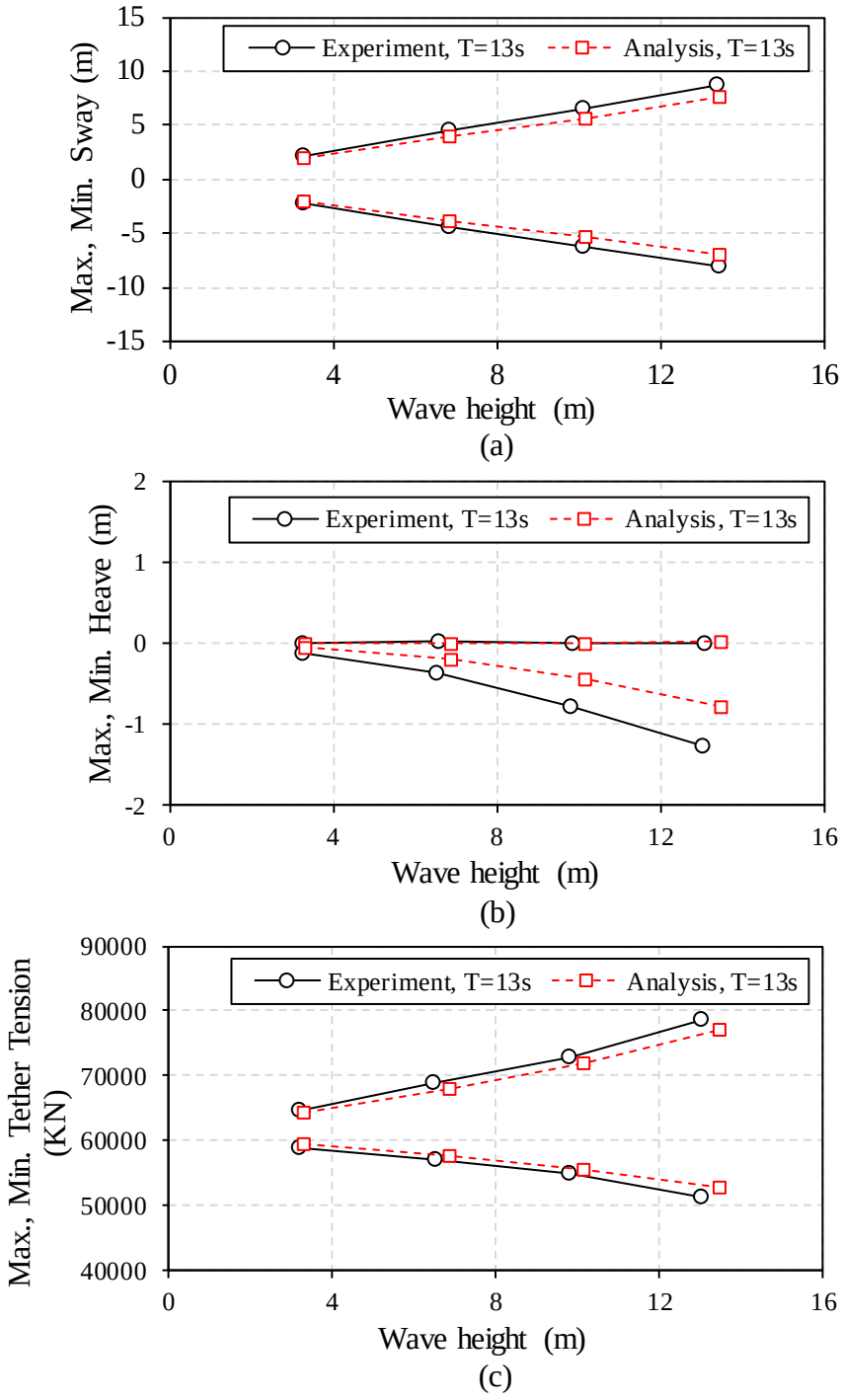

Figure 3.6. SFT response as function of wave height (T=13 s)

(a) sway motion; (b) heave motion; (c) tether tension

In most cases, the experimental and analytical results agree very well. However, inconsistent results were found for some high wave height or high wave periods, such as Figure 3.6 (b). The error is expected because of the assumption of drag coefficient, considering the nonlinearity of the wave, and additional scattering effect according to the structure in the analysis model. The horizontal displacement mainly dealt with in this study matches well, so the analysis model can be expected to reflect the actual movement well.

CHAPTER 4

PARAMETER STUDY

In this study, the behavioral characteristics according to the major design parameters of SFT were identified through the verified analysis technique. Considering that research on various parameters through scaled wave flume experiments is difficult in terms of cost and time, the behavioral characteristics were analyzed by adjusting the parameters within various possible ranges using an analysis program. Characteristics of waves (height and period), buoyancy weight ratio (BWR), tunnel clearance, and mooring line incline angle were used as main parameters. The behavior of the SFT was evaluated depending on these variables.

4.1 Parameter's range selection

4.1.1 Considered wave cases

First, an appropriate selection criterion for the wave height period and wave height were established. It was assumed that the SFT design was carried out on the southern coast of South Korea. Three-year wave measurement data of the Yeosu area were extracted from WINK [24] and analyzed (Figure 4.1). The wave period is also displayed as a histogram shown in Figure 4.2.

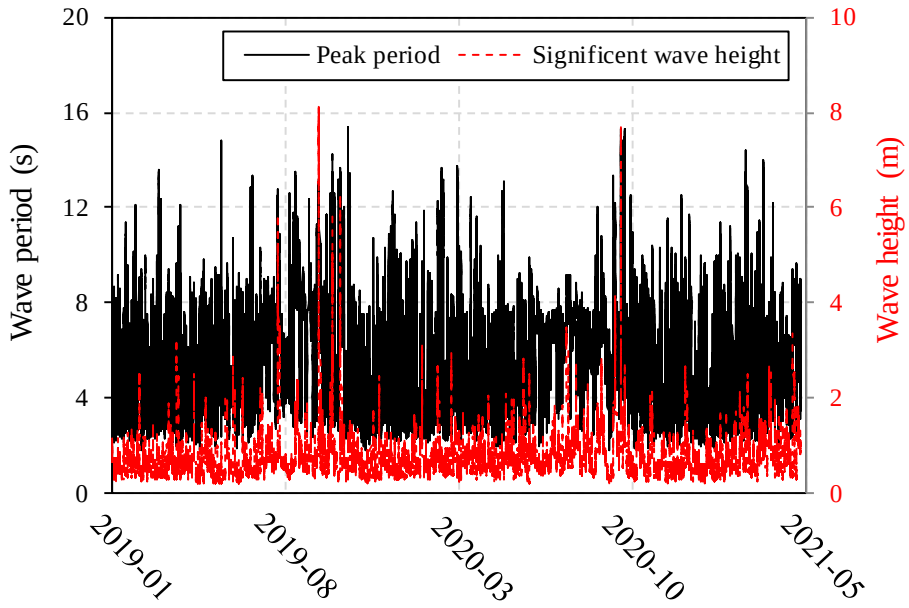

Figure 4.1. 3 years wave measurement data of Yeosu area

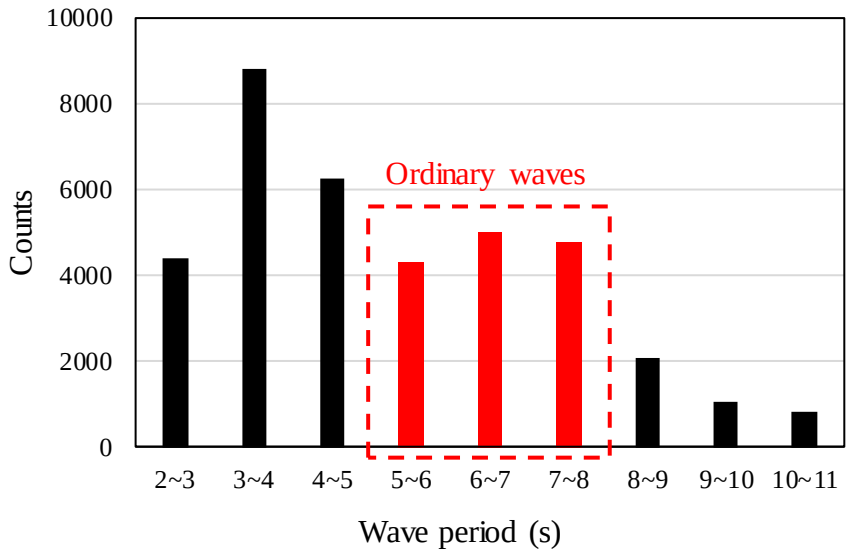

Figure 4.2. Wave period Histogram for the past 3 years

For waves with a period of less than 5 seconds on the Histogram, the structure response displacement is small enough to be ignored. Wave with a period of 5 to 8 seconds which is not small but frequent, is considered ordinary waves. The following wave does not cause extreme displacement of the structure, but it may cause fatigue failure at high frequencies.

Figure 4.3 shows a 50-year return period maximum wave period based on the National Deep-Sea Design Wave Estimation Report [25]. A wave period of 12 to 16 seconds was defined as the high energy wave case based on the data.

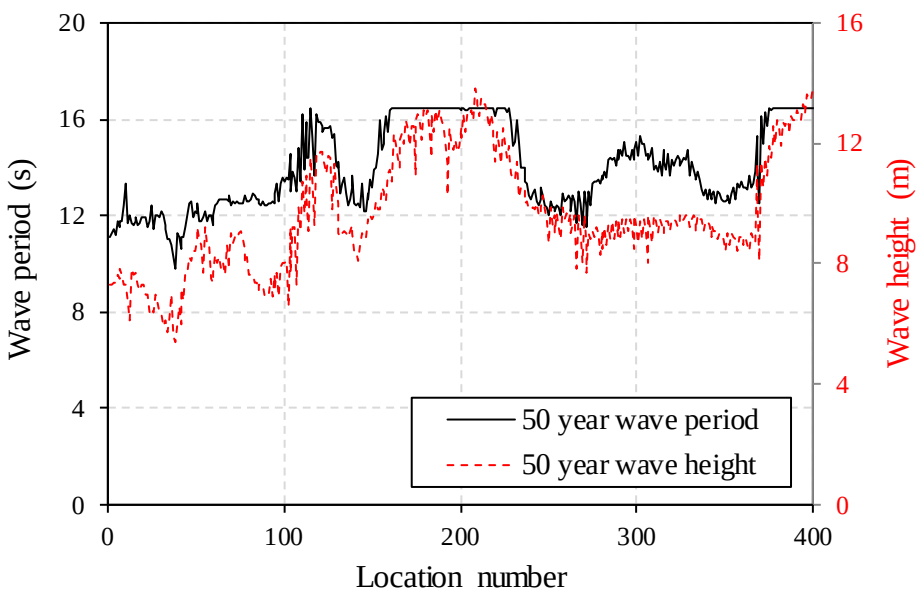

Figure 4.3. 50-years recurrence period maximum wave period and wave height by locations.

Therefore, the wave period, an independent variable, was defined as 6 to 16 seconds (Table 4.1). The remaining variables (wavelength and wave height) were determined according to the distribution relationship in Equation (3.1) and the wave height-period relationship in Figure 4.4. Here, the wave height-period relational expression was derived through regression analysis of posterior data.

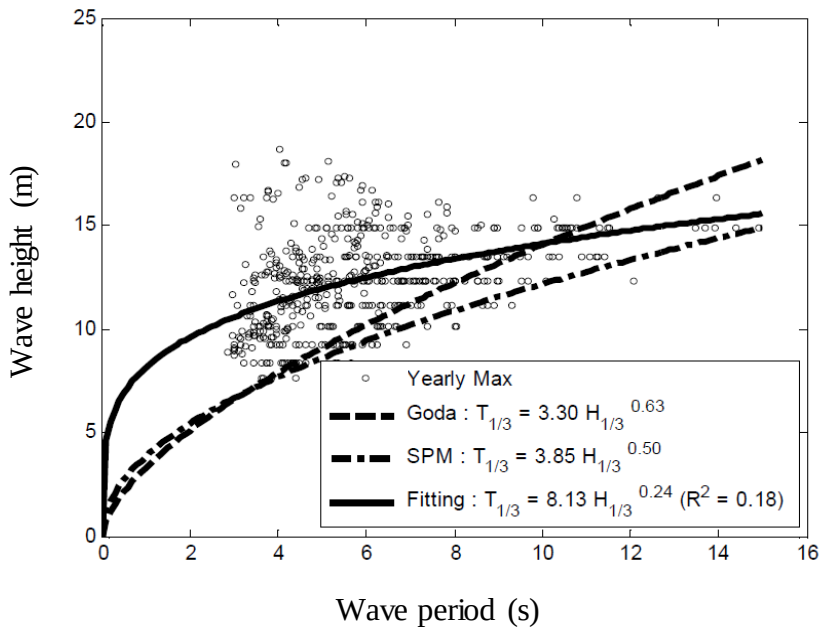

Figure 4.4. Wave period-height relationship [23]

Table 4.1. Parameters for different regular waves

Case	Wave period, T (s)	Wave length, λ (m)	Wave height, H (m)
Wave-1	6	56	0.7~3.0
Wave-2	8	100	1.3~5.3
Wave-3	10	156	2.0~8.3
Wave-4	12	223	2.9~11.8
Wave-5	14	297	3.9~15.7
Wave-6	16	373	4.9~19.8

4.1.2 The considered range for buoyancy weight ratio

The following is a selection of parameter ranges related to the structural system. First, as shown in Table 4.2, the case according to the BWR was selected. Since the change in tunnel diameter is not considered in this study, BWR changes only by the structure's weight. BWR range was confirmed as 1.5 to 6, considering the design of tunnel materials from steel to lightweight concrete.

Table 4.2. Analysis cases for BWR

Case	BWR	Clearance (m)	Tether incline angle (°)
B-1	1.5	20	90
B-2	1.75		
B-3	2		
B-4	2.25		
B-5	2.5		
B-6	2.75		
B-7	3		
B-8	3.5		
B-9	4		
B-10	4.5		
B-11	5		
B-12	5.5		
B-13	6		

4.1.3 The considered range for clearance

The clearance, also called a draft, was selected to be 15 m or more, considering the ship's operating depth. In this study, the water depth of the target sea area was assumed to be 100 m, and it was confirmed that hydrostatic pressure on the tunnel was not a problem. Consequently, clearance was evaluated from 15 m to 60 m.

Table 4.3. Analysis cases clearance

Case	BWR	Clearance (m)	Tether incline angle (°)
C-1	2	15	90
C-2		20	
C-3		25	
C-4		30	
C-5		35	
C-6		40	
C-7		45	
C-8		50	
C-9		55	
C-10		60	

4.1.4 The considered range for tether incline angle

The mooring line inclination angle, which is the initial angle between the mooring line and the x-axis at equilibrium, is a major design variable because it greatly affects the horizontal and vertical stiffness of the SFT. From a static point of view of the structural system, as the inclination angle increases, the horizontal stiffness increases while the vertical stiffness decreases. Structural rigidity varies greatly depending on the inclination angle of the mooring line, so it was confirmed by analyzing in a wide range as 45°~90° (Table 4.4).

Table 4.4. Analysis cases for tether incline angle

Case	BWR	Clearance (m)	Tether incline angle (°)
I-1	2	20	90
I-2			75
I-3			60
I-4			45

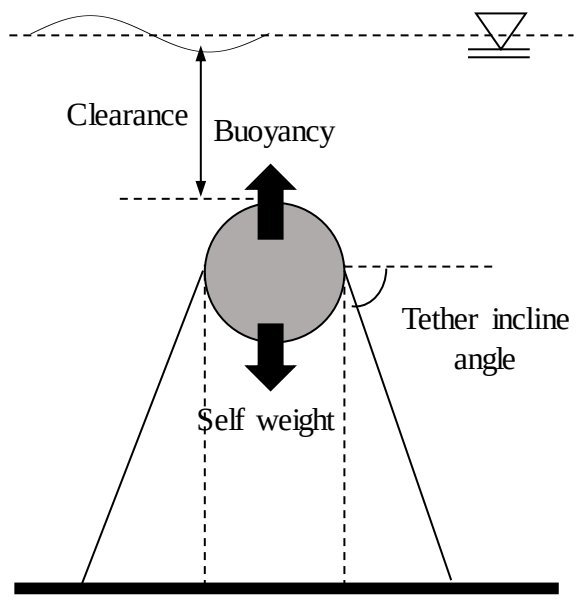

Figure 4.5. Main structural parameters for SFT

4.2 Wave characteristics case study

The following is the result for performing parameter study using a numerical analysis program. The first case study is the behavioral characteristics of the SFT according to the wave characteristics. According to the Airy wave theory, the velocity potential is proportional to the height and period of the wave (Equation (2.5)). Therefore, the structural response can be expected to increase as the wave height and period increase. Figure 4.6 shows the maximum and minimum displacement values according to wave period and height. As expected, it can be seen that the structure response increases as the wave height and period increase.

In Figure 4.6 (a), it can be seen that there is a difference between the maximum and minimum values of sway instead of being symmetric. Even though the velocity and acceleration of the wave particles are sinusoidal, the cause of this difference is expected to be the influence of the absolute value in the drag term of Morison's Equation.

In addition, it can be seen that the vertical fluctuation is relatively smaller than the lateral fluctuation. The reason is that the mooring lines constrain the SFT only in the vertical direction, making it vulnerable to lateral loads. In the case of vertical fluctuation, only the minimum value was large. This indicates that tethers have no elastic deformation, and the Vertical motion is accompanied by horizontal motion.

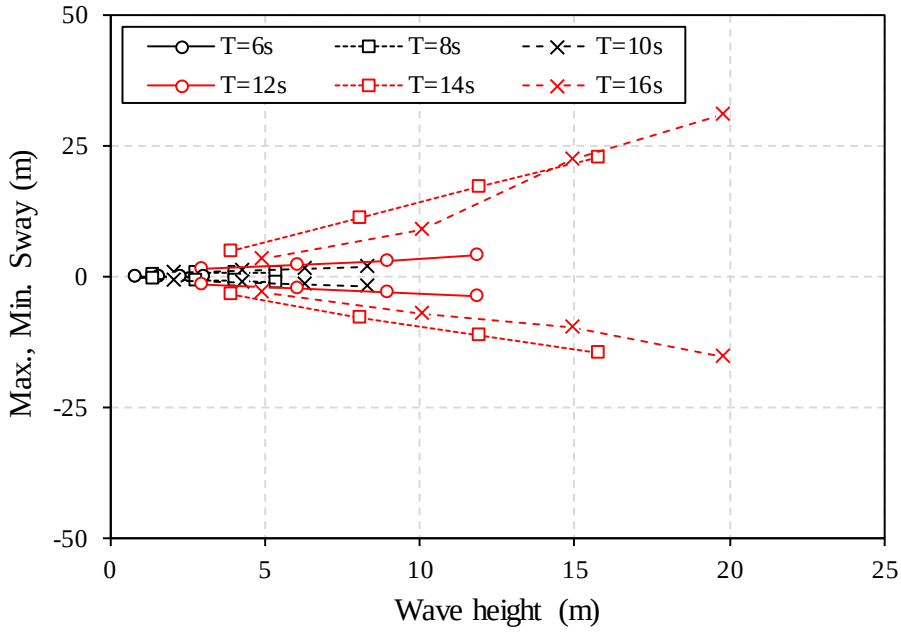

(a)

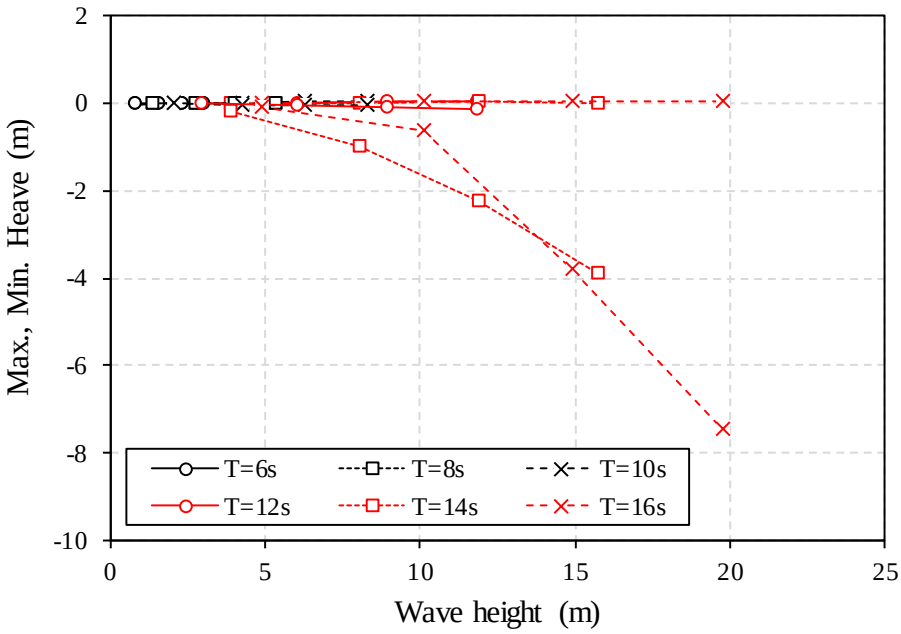

(b)

Figure 4.6. Response according to different wave characteristics (a) sway motion; (b) heave motion

4.3 Buoyancy-weight ratio case study

Next, the behavioral characteristics of the SFT according to the buoyancy-self-weight ratio were evaluated. As the self-weight of the tunnel decreases, the BWR increases, and the mooring line tension also increases. This leads the structural lateral stiffness to increase. However, according to Figure 4.7 (a), it can be seen that the response is greatly amplified in a particular section. Similarly, the heave motion in Figure 4.7 (b) is greatly amplified in the same BWR section.

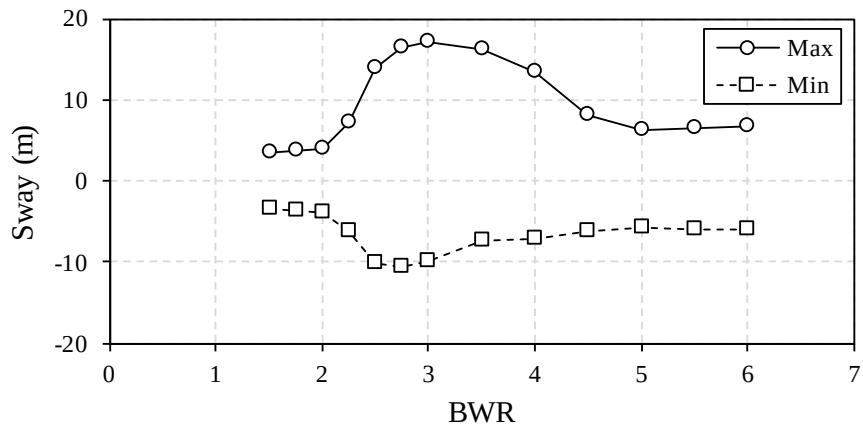

(a)

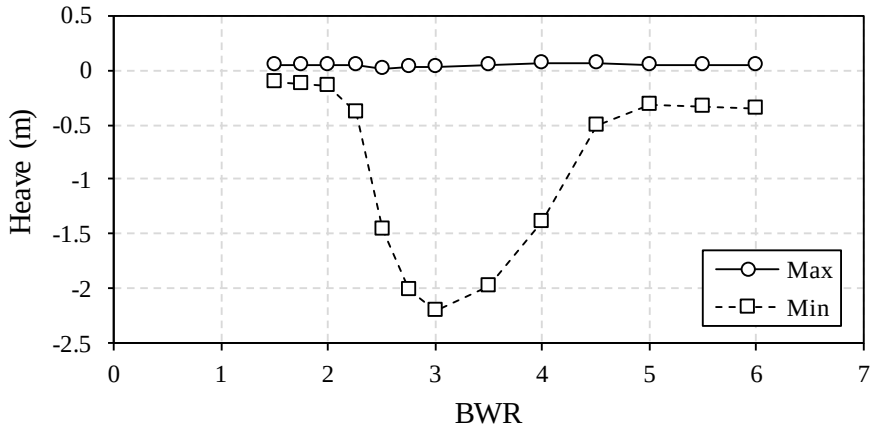

(b)

Figure 4.7. Structure response under different BWR (a) sway; (b) heave

In order to investigate the reason for this structure response amplification, the lateral displacement with time is plotted for BWR 2, 3, 4, and 5 (Figure 4.8). For BWR 3 and 4, where the response is amplified, frequency components other than the wave period are detected.

Also, based on the lateral displacement over time, the natural structure frequency that changes in real-time can be calculated, as shown in Figure 4.9. For BWR 3 and 4, it can be seen that there is a moment when the natural frequency of the structure coincides with the frequency of the wave.

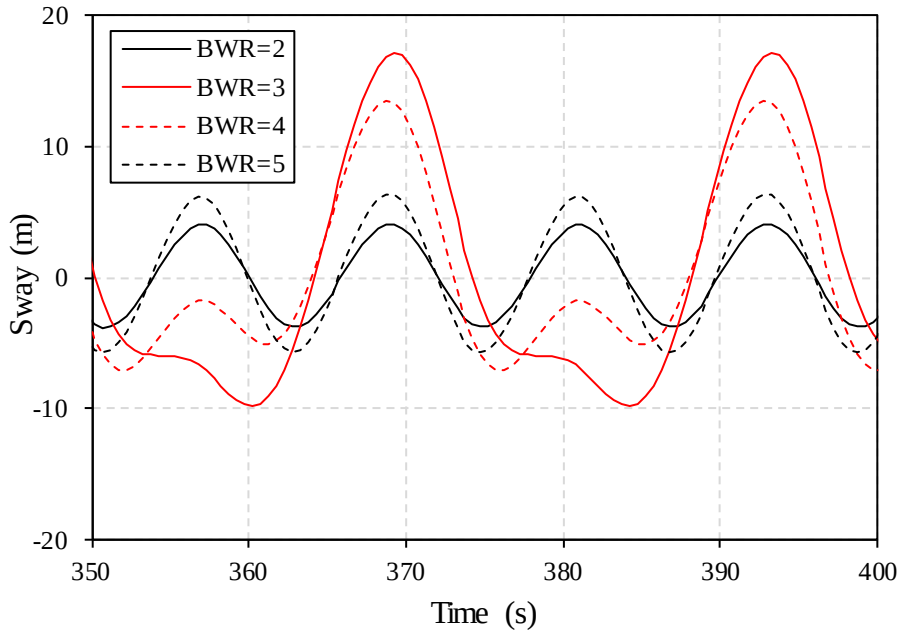

Figure 4.8. Dynamic response with different BWR versus time

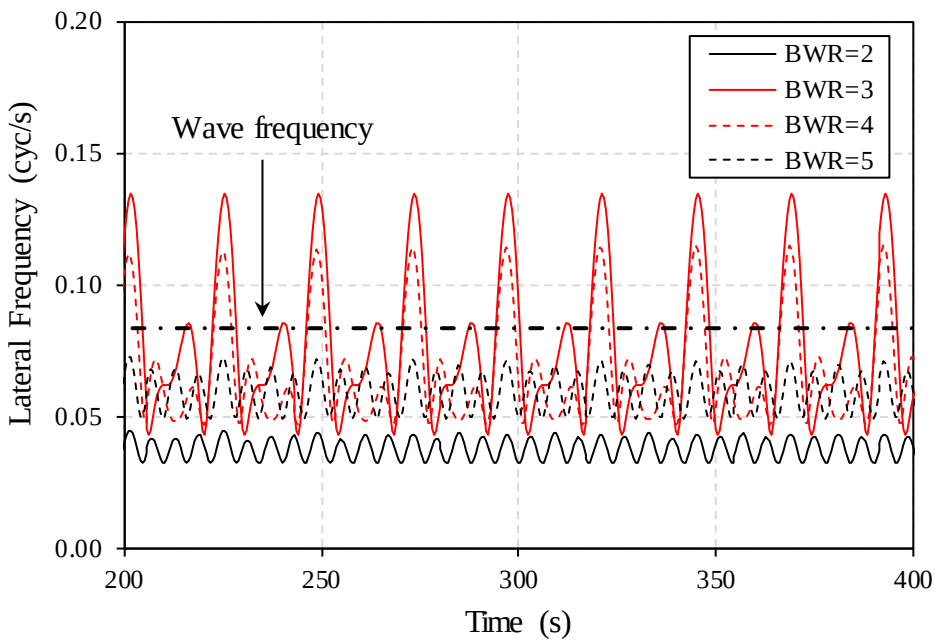

Figure 4.9. The natural frequency with different BWR versus time

In order to intuitively check the following phenomena, the structure's natural frequency is expressed as a range for each BWR case. As shown in Figure 4.10 (a), if the natural frequency of the structure is calculated without considering structure displacement, it is far from the natural frequency of the wave.

However, if the natural frequency range is calculated considering the displacement of the real-time structure obtained from the analysis result, it can be confirmed that there is a section consistent with the natural frequency of the wave, as shown in Figure 4.10 (b). The corresponding BWR section matches the response amplification section in Figure 4.7.

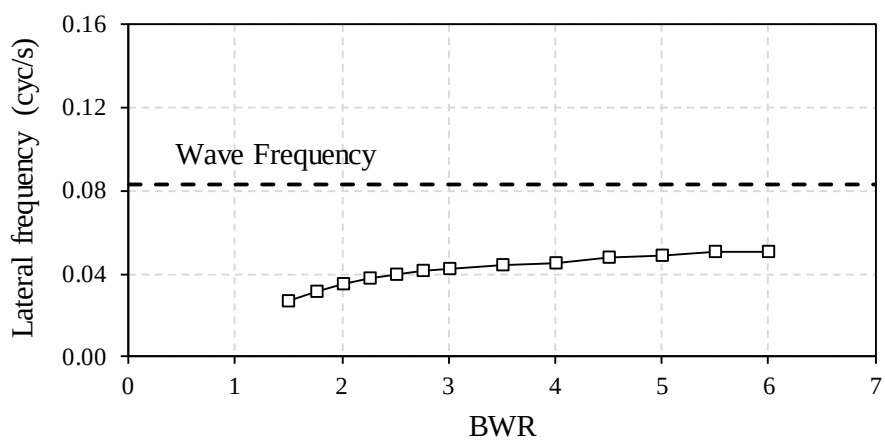

(a)

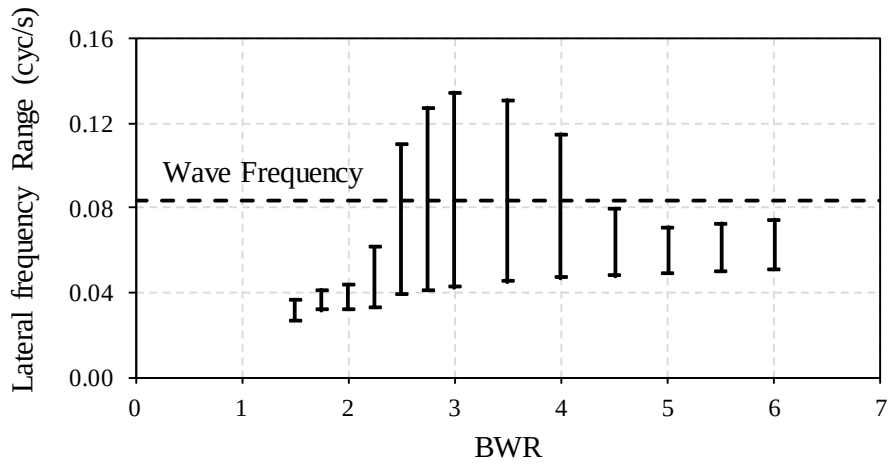

(b)

Figure 4.10. System natural frequency range with different BWR

(a) considering $u = 0$; (b) considering $u \neq 0$

4.4 Clearance case study

A case study was conducted according to the tunnel clearance. According to the Airy linear wave theory, the tunnel becomes farther from the sea level as the clearance increases, so the absolute wave force decreases. However, it can be seen from Figure 4.11 that the response amplification section occurs similarly to the results shown in the previous BWR case study.

To explain why the structural response is amplified, the lateral displacement over time is plotted as shown in Figure 4.12. It can be confirmed that frequency components other than the wave period are detected for clearance 40 and 45 cases. Also, for these particular cases, which is the case

where the peak occurs, there is a moment when the natural frequency of the fluctuating structure coincides with the wave frequency. (Figure 4.13)

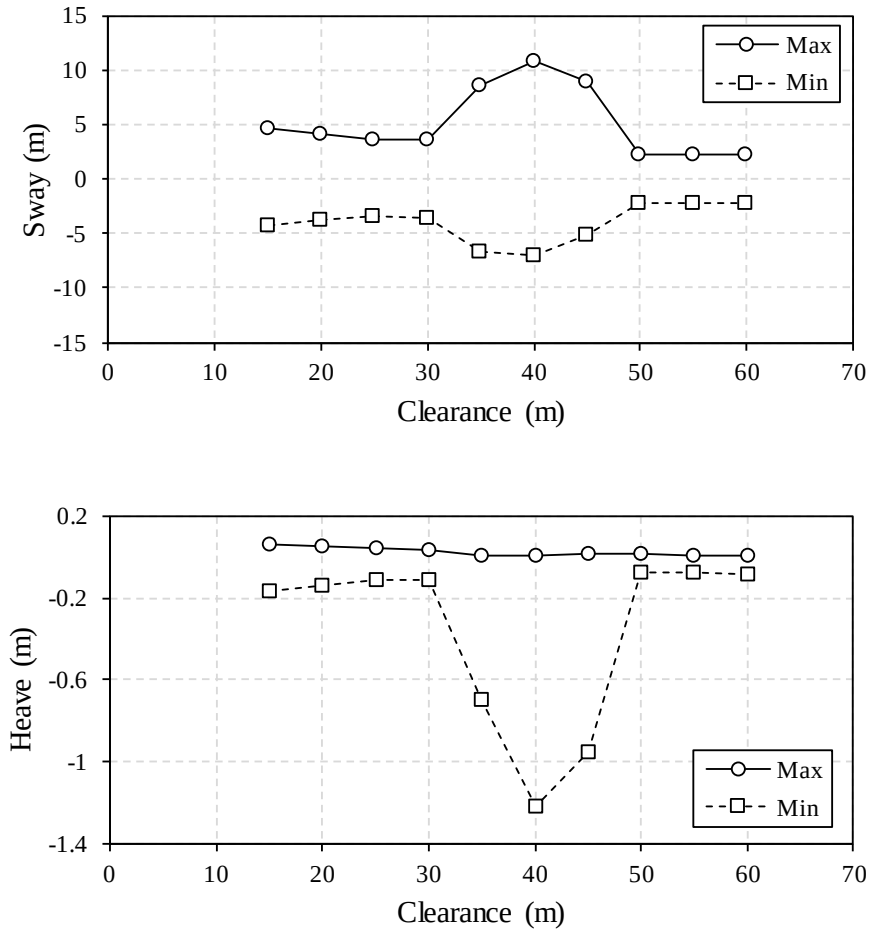

Figure 4.11. Structure response under different clearance (a) sway; (b) heave

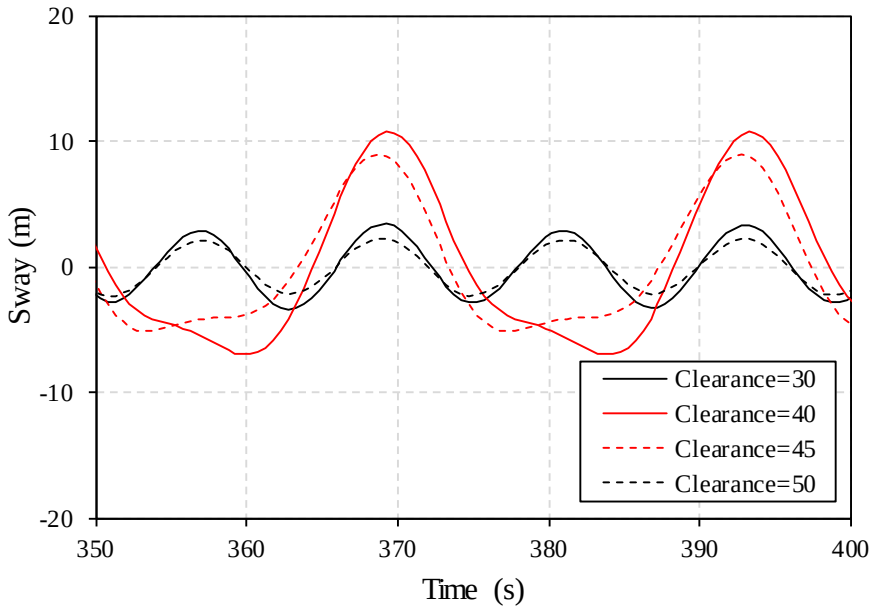

Figure 4.12. Dynamic response with different clearance versus time

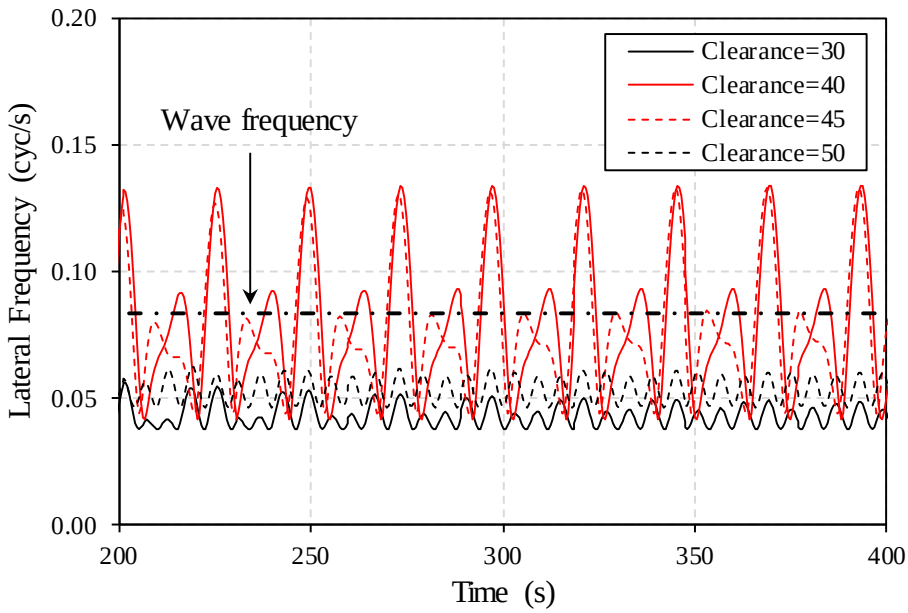

Figure 4.13. The natural frequency with different clearance versus time

The natural frequencies of the structures were expressed as ranges for each clearance case. By Figure 4.14 (b), it can be confirmed that there is a section that matches the natural frequency of the wave, and this can be obvious only when the fluctuating natural frequency is calculated with real-time structure displacement.

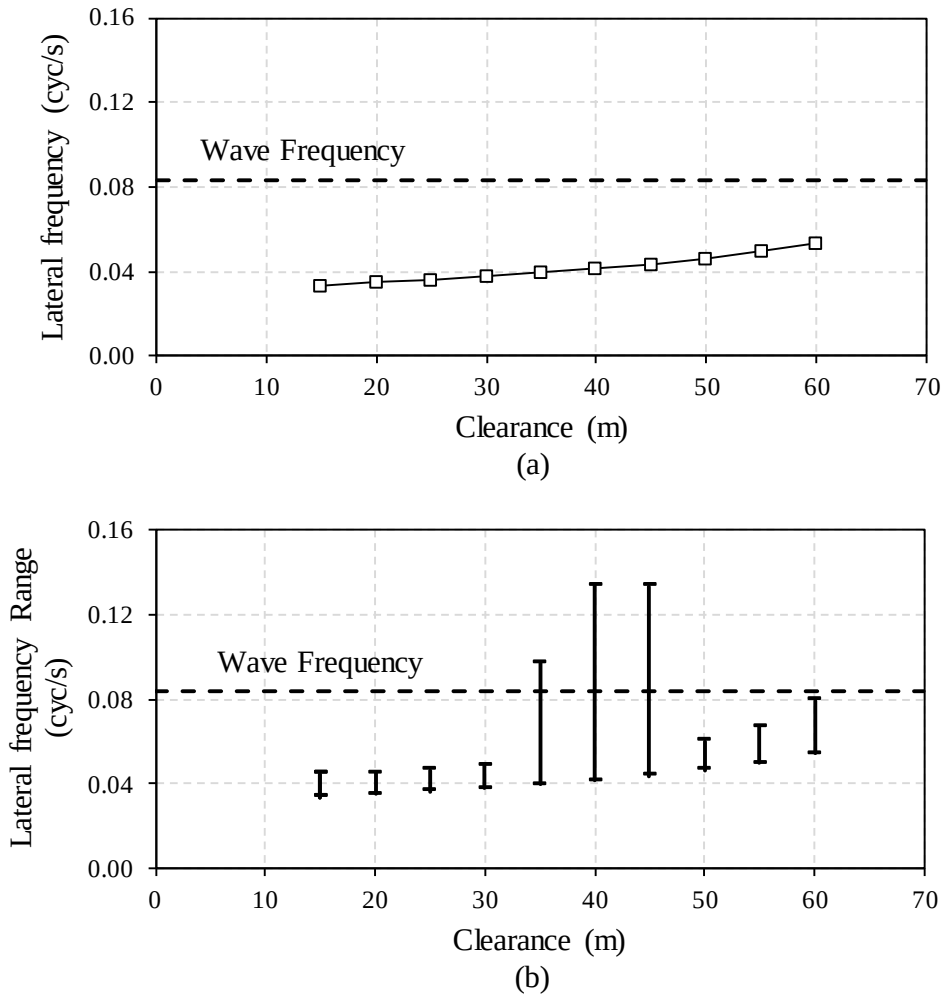

Figure 4.14. System natural frequency range with different clearance

(a) considering $u = 0$; (b) considering $u \neq 0$

4.5 Tether incline angle case study

Finally, a parameter study according to the angle of the mooring line was conducted. As shown in Figure 4.15 (b), the heave motion of the tunnel is greatly amplified below 60 degrees. Also, the tension of the mooring line, as shown in Figure 4.15 (c), approaches near zero at 45 degrees. Losing all of the tether tension can be very dangerous because this can lead to dynamic instability of SFT due to the tether stack.

Therefore, it can be seen that the displacement of the structure does not tend to decrease even when the mooring line angle is reduced, and it can be seen that the vertical displacement and the mooring line tension rapidly increase around 45 degrees.

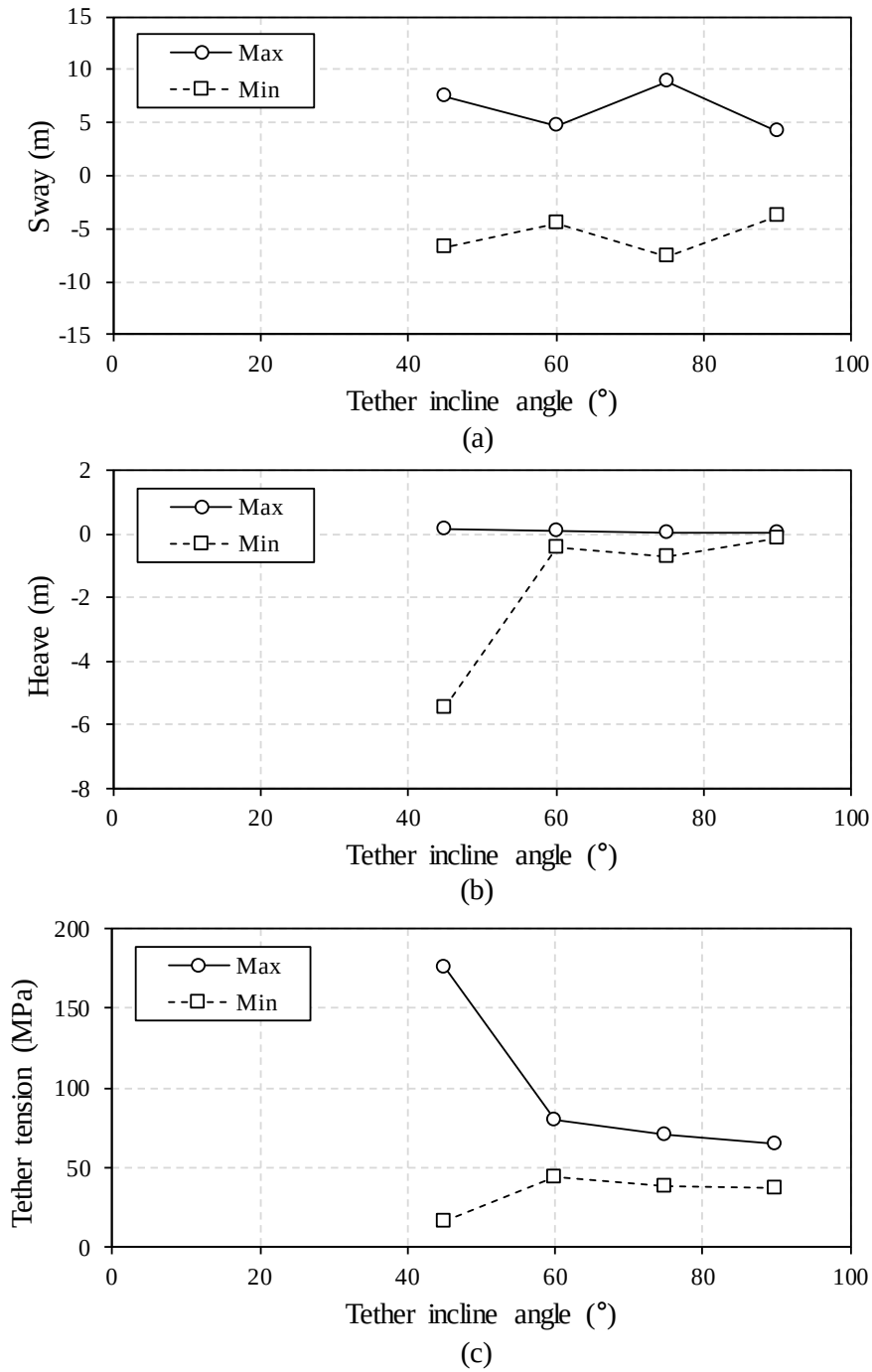

Figure 4.15. Structure response under different tether incline angle

(a) sway; (b) heave; (c) tether tension

CHAPTER 5

CONCLUSION

The objectives of this dissertation were to first theoretically understand wave-structure interaction and propose a verified numerical model that reflects the actual movement of SFT. The second objective was to examine the structural response under wave load with different structural parameters. The following conclusions were made based on the previous chapters.

(1) Based on Airy linear wave theory and Morison's Equation, wave load was established, and the governing Equation of the SFT system was also derived.

(2) The numerical model was validated by comparing the analysis result with the theoretical solution and scaled experiment result.

(3) The effect of key design parameters (Buoyancy weight ratio, clearance, tether incline angle) on the performance of SFT under wave load is presented.

(4) For the particular BWR range (BWR: 2 ~ 4), SFT response becomes severe. Since the structural lateral stiffness is motion-dependent by the P-delta effect, the fluctuating natural frequency overtime is calculated using the pre-analyzed displacement result. It can be

confirmed that the section where the fluctuating structural natural frequency and the wave frequency overlaps makes SFT response amplified.

(5) For clearance, the response amplification region appeared for 35 m ~ 45 m. The cause appeared to be the same as previous results.

(6) For below 45 degrees of mooring line angle, the vertical displacement and the mooring line tension rapidly increased.

(7) When designing an SFT, extreme structural displacement may occur even if the wave frequency and the natural frequency of the structure are not close. Thus, the structure's fluctuating natural frequency should be properly considered for such SFTs.

REFERENCE

[1] Jin, C., & Kim, M. (2021) "The Effect of Key Design Parameters on the Global Performance of Submerged Floating Tunnel under Target Wave and Earthquake Excitations" CMES-COMPUTER MODELING IN ENGINEERING & SCIENCES, 128(1), 315-337.

[2] Kim, S., Park, W. S., & Won, D. H. (2016) "Hydrodynamic analysis of submerged floating tunnel structures by finite element analysis" Journal of the Korean Society of Civil Engineers, 36(6), 955-967.

[3] Long, X., Ge, F., & Hong, Y. (2015) "Feasibility study on buoyancy–weight ratios of a submerged floating tunnel prototype subjected to hydrodynamic loads" Acta Mechanica Sinica, 31(5), 750-761.

[4] Chen, X., Chen, Z., Cai, S., Xu, W., Zhuo, X., Lv, J., & Zhao, J. (2020) "Numerical investigation of dynamic responses and mooring forces of submerged floating tunnel driven by surface waves" Scientific Reports, 10(1), 1-19.

[5] Oh, S. H., Park, W. S., Jang, S. C., Kim, D. H., & Ahn, H. D. (2013). "Physical experiments on the hydrodynamic response of submerged floating tunnel against the wave action" In Proceedings of the 7th international conference on Asian and Pacific Coasts (APAC 2013) (pp. 582-587).

[6] Oh, S. H., Park, W. S., Jang, S. C., & Kim, D. H. (2013) "Investigation on the behavioral and hydrodynamic characteristics of submerged floating tunnel based on regular wave experiments" Journal of the Korean Society of Civil Engineers, 33(5), 1887-1895.

[7] Yang, Z., Li, J., Zhang, H., Yuan, C., & Yang, H. (2020) "Experimental study on 2D motion characteristics of submerged floating tunnel in waves" Journal of Marine Science and Engineering, 8(2), 123.

[8] Won, D., Seo, J., & Kim, S. (2021) "Dynamic response of submerged floating tunnels with dual sections under irregular waves" Ocean Engineering, 241, 110025.

[9] Zhang, H., Yang, Z., Li, J., Yuan, C., Xie, M., Yang, H., & Yin, H. (2021) "A global review for the hydrodynamic response investigation method of submerged floating tunnels" Ocean Engineering, 225, 108825.

[10] Paik, I. Y., Oh, C. K., Kwon, J. S., & Chang, S. P. (2004) "Analysis of wave force induced dynamic response of submerged floating tunnel" KSCE Journal of Civil Engineering, 8(5), 543-550.

[11] Kunisu, H. (2010) “Evaluation of wave force acting on Submerged Floating Tunnels” Procedia Engineering, 4, 99-105.
[12] Cifuentes, C., Kim, S., Kim, M. H., & Park, W. S. (2015) “Numerical simulation of the coupled dynamic response of a submerged floating tunnel with mooring lines in regular waves” Ocean Systems Engineering, 5(2), 109-123.
[13] Long, X., Ge, F., Wang, L., & Hong, Y. (2009) “Effects of fundamental structure parameters on dynamic responses of submerged floating tunnel under hydrodynamic loads” Acta Mechanica Sinica, 25(3), 335-344.
[14] Luo, W., Huang, B., Tang, Y., Ding, H., Li, K., Cheng, L., & Ren, Q. (2022) “Numerical Simulation of Dynamic Response of Submerged Floating Tunnel under Regular Wave Conditions” Shock and Vibration, 2022.
[15] Deng, S., Ren, H., Xu, Y., Fu, S., Moan, T., & Gao, Z. (2020) “Experimental study of vortex-induced vibration of a twin-tube submerged floating tunnel segment model” Journal of Fluids and Structures, 94, 102908.
[16] Deng, S., Ren, H., Xu, Y., Fu, S., Moan, T., & Gao, Z. (2020) “Experimental study on the drag forces on a twin-tube submerged floating tunnel segment model in current” Applied Ocean Research, 104, 102326.
[17] Lin, H., Xiang, Y., Yang, Y., & Chen, Z. (2018) “Dynamic response analysis for submerged floating tunnel due to fluid-vehicle-tunnel interaction” Ocean Engineering, 166, 290-301.
[18] Seo, S. I., Mun, H. S., Lee, J. H., & Kim, J. H. (2015). Simplified analysis for estimation of the behavior of a submerged floating tunnel in waves and experimental verification. Marine Structures, 44, 142-158.
[19] Won, D. H., & Kim, S. (2017). Dynamic Instability of Submerged Floating Tunnels due to Tendon Slack. Journal of Korean Society of Steel Construction, 29(6), 401-410.
[20] Hong, Y., & Ge, F. (2010). Dynamic response and structural integrity of submerged floating tunnel due to hydrodynamic load and accidental load. Procedia Engineering, 4, 35-50.
[21] Jakobsen, B. (2010). Design of the Submerged Floating Tunnel operating under various conditions. Procedia Engineering, 4, 71-79.
[22] Mazzolani, F. M., Landolfo, R., Faggiano, B., Esposto, M., Perotti, F., & Barbella, G. (2008) “Structural analyses of the submerged floating tunnel prototype in Qiandao Lake (PR of China)” Advances in structural engineering, 11(4), 439-454.

[23] Oh, J. H., Suh, K. D., & Lee, D. Y. (2009) “Relationship between significant wave height and period in coasts of Korean Peninsula” In Proceedings of the Korean Society of Coastal and Ocean Engineers Conference (pp. 69-72).

[24] 정원무, 오상호, 류경호, 백종대, & 최일훈. (2018) “전국파랑관측자료 제공시스템 WINK 구축” 한국해안·해양공학회논문집, 30(6), 326-336.

[25] 해양수산부 (2019) 전국 심해설계파 산출 보고서

국 문 초 록

본 연구에서는 계류선이 있는 부유식 수중 터널의 유탄성 거동 해석을 수행하였고, 주요 매개변수가 파랑하중에 의한 동적 응답에 미치는 영향을 평가하였다. 파력을 산정하기 위해서는 Airy 선형파 이론과 Morison 방정식이 사용되었다. 또한, 부유식 수중 터널의 수치 모델은 선행 연구의 조파수조 실험 결과와 비교함으로써 검증하였다. 파랑 하중이 가해질 때, 수중 터널의 주요 설계 변수인 부력-중량비, 터널의 흘수, 계류선의 경사각이 동적 거동에 미치는 영향이 평가되었다. 결과적으로, 부유식 수중 터널의 고유진동수와 파진동수가 근접하지 않았음에도 불구하고, 매개변수의 특정 범위에 대해 구조물 응답 증폭 현상이 관찰되었다. 이 증폭 현상은 P-delta 효과에 의해 시간에 따라 변동하는 고유 진동수로 인한 것으로 밝혀졌다.

주요어: 부유식 수중 터널, 유탄성 거동 해석, 부력-중량비, 흘수, 구조물 응답 증폭 현상

학번: 2020-29808